Waveform Design and Receive Processing for Nonrecurrent Nonlinear FMCW Radar

John Jakabosky and Shannon D. Blunt
Radar Systems Lab
University of Kansas
Lawrence, KS

Braham Himed
Sensors Directorate
Air Force Research Laboratory
Dayton, OH

***Abstract* – A spectral shaping optimization scheme is used to design the autocorrelation response of individual segments of a nonrecurrent nonlinear FMCW waveform denoted as Pseudo-Random Optimized FMCW (or PRO-FMCW). Because each waveform segment is unique, the range sidelobes do not combine coherently during Doppler processing thereby providing further sidelobe suppression. The PRO-FMCW waveform can be viewed as a specific instantiation of FM noise radar where the constant amplitude permits maximum power efficiency. A segmented approach to processing the received data is used to reduce processing time and complexity. Measured results from hardware implementation are provided to demonstrate the efficacy of the proposed approach.**

I. INTRODUCTION

The notion of changing the waveform on a pulse-to-pulse basis during the coherent processing interval (CPI) can be traced back to stepped frequency waveforms to increase overall bandwidth and complementary coding (see [1, Chap. 9] and references therein). With the emergence and continued advancement of high-fidelity waveform generation this concept of pulse agility or pulse diversity has also been examined as a way to increase the dimensionality of the radar emission for diverse purposes such as the extension of the maximum ambiguous range [2,3], embedded communication on transmit [4,5], and joint delay-Doppler imaging [6], all being examples of waveform diversity [7-9].

One could likewise view noise radar as a continuous wave (CW) instantiation of this same principle as the waveform is always changing (see [10] and references therein). Because it mimics random noise, such a radar inherently possesses a low probability of intercept (LPI) and has no range ambiguities, though the typical requirement for amplitude modulation tends to limit noise radar to short range applications. Alternatively, it has been shown [11] that randomly modulating phase or frequency has advantages over traditional complex amplitude modulated noise radar in terms of range resolution as well as the ability to use power efficient amplifiers since the resulting phase/frequency modulated waveform is constant modulus.

An important implication of this changing waveform structure is that the range sidelobes likewise change on a pulse-to-pulse basis (or processing segment-to-segment for CW). This sidelobe modulation effect produces a range sidelobe floor when performing Doppler processing such that, in the presence of strong scatterers (e.g. clutter), these sidelobes can wash out the scene. Since traditional clutter filtering only removes the mainlobe response of the scatterer, these modulated sidelobes remain. Sophisticated adaptive filtering approaches may address these modulated sidelobes [2,3,6], though at a high computational cost. The alternative is to embrace the large dimensionality by maximizing the overall time-bandwidth product and exploiting the lack of sidelobe coherence, which is essentially how noise radar operates.

The approach proposed here employs the random FM structure, albeit with the inclusion of spectral shaping as suggested in [11] whereby the power spectral density is constrained to a Gaussian shape which likewise translates into a Gaussian-shaped autocorrelation with low range sidelobes. This spectral shaping procedure is inspired by the iterative approaches described in [12,13], though instead of avoiding spectral regions the goal here to match to the Gaussian power spectral density. By initializing each FMCW segment with a random phase signal followed by Gaussian spectral shaping, low range sidelobes can be achieved that likewise are not coherent over the segments used for Doppler processing. This nonrecurrent nonlinear FM continuous waveform, denoted as Pseudo-Random Optimized FMCW (PRO-FMCW), realizes a power efficient emission due to constant amplitude, good spectral containment due to the spectral shaping, is range unambiguous, and achieves very low sidelobe levels given a sufficiently long CPI for receive processing.

The optimization process is amenable to real-time operation given sufficient processing capability. Aside from the need to account for the convolutional tails that arise for the CW waveform structure, standard matched filter pulse compression and Doppler processing (including clutter cancellation) can be applied to the received data. Further, sliding window Doppler processing can be used to provide a rapid refresh of the range-Doppler response.

II. SPECTRAL-SHAPING OPTIMIZATION

The spectral shaping design developed here for the individual waveform segments is the same as that developed in [14], although here constant modulus is enforced and each waveform segment is randomly (and independently) initialized prior to the spectral shaping optimization. The overall approach is as follows: a random phase signal is generated, this signal is optimized to produce a segment of the waveform with a prescribed power spectral density, and then the beginning of this segment is phase-aligned with the end of the previous segment. The nonrecurrent, nonlinear FMCW waveform is thus constructed in piece-wise fashion where receive processing is likewise performed on the individual segments.

This work was supported by a subcontract with Booz, Allen and Hamilton for research sponsored by the Air Force Research Laboratory (AFRL) under Contract FA8650-11-D-1011.

The spectral shaping optimization is an iterative process involving the sequential application of

$$r_{k+1,m}(t) = \mathbb{F}^{-1}\left\{|G(f)|\exp\left(j\angle\mathbb{F}\left\{p_{k,m}(t)\right\}\right)\right\} \quad (1)$$

and

$$p_{k+1,m}(t) = w(t)\exp\left(j\angle r_{k+1,m}(t)\right) \quad (2)$$

where $p_{0,m}(t)$ is the initial randomly generated phase signal for the mth segment, $w(t)$ is a rectangular window of length T, $|G(f)|^2$ is the desired power spectral density, $\mathbb{F}$ and $\mathbb{F}^{-1}$ are the Fourier and inverse Fourier transforms, respectively, and $\angle(\bullet)$ extracts the phase of the argument. This process is repeated for K iterations to obtain the mth optimized signal $p_{K,m}(t)$. To prevent abrupt phase jumps, the mth optimized signal is phase rotated to yield the mth waveform segment as

$$s_m(t) = \exp\left(j\phi_{\text{end},m-1}\right)p_{K,m}(t) \quad (3)$$

where $\phi_{\text{end},m-1}$ is the ending phase for the $(m-1)$th segment.

This optimization approach can be implemented efficiently using FFTs and IFFTs. Leveraging general purpose GPU (GPGPU) computation and parallel processing, it is possible to generate the optimized segments in real-time.

III. Receive Processing

The receive echoes are organized for processing in the same manner as the transmitted waveform segments. To account for the convolutional tails in the matched filtering of this CW signal, portions of the (m–1)th and (m+1)th segments are included in the data to which the mth matched filter is applied (Fig. 1). The mth matched filter is the time-reversed complex conjugate of the waveform segment defined in (3).

This process is repeated for each segment. Doppler processing via FFT of M contiguous pulse compressed segments provides a range-Doppler map that can be updated in a sliding window manner as each new segment is pulse compressed. Standard clutter cancellation can also be incorporated into this sliding window Doppler processing.

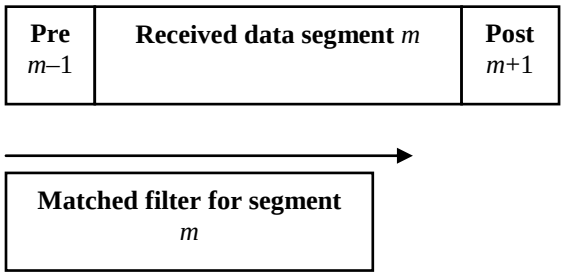

Fig. 1. Pulse compression for the mth segment

Figure 1 shows that the matched filter is applied to the combined pre, post, and current segments. Only a small number of samples from the previous segment are needed. The portion of the (m+1)th segment that is required is determined by the length of the desired range interval. For instance, to capture 750 meters of range data at a sampling rate of 200 MS/s, 1000 samples or 5 μs from the (m+1)th segment would be required. If the desired range interval is greater than the length of a segment, additional segments can be appended as required. Since the echoes generated by a segment also include the reflected responses from previous segments, interference can be a problem. The cross-correlation sidelobe interference increases as more samples from the (m+1)th segment are included. Thus the minimum required to image the desired range should be used.

IV. Laboratory Measurements

To verify the performance of the PRO-FMCW design, a waveform with a length of T_w = 200 milliseconds was produced comprising $M = 10^4$ segments of length T = 20 μs. This waveform has a design bandwidth of B = 80 MHz and was sampled at 200 Mega-samples per second. Each segment possesses a time-bandwidth product of 1600 while the total processing gain is 1.6×10^7 or 72 dB.

The optimization of each segment was performed using a Gaussian power spectral density which produces both good spectral roll-off and low autocorrelation sidelobes. Each segment was optimized using (1) and (2) for K = 500 iterations. The initialization for each segment optimization was a random sequence of 1600 phase values drawn from a uniform distribution on [–π, π] and subsequently implemented using the polyphase-coded FM (PCFM) framework from [15].

The resulting waveform was implemented in a hardware testbed using a Tektronix AWG70002 waveform generator, a Rohde & Schwarz FSW spectrum analyzer to capture the echo response, and a pair (one for TX, one for RX) of vertically polarized patch array antennas with effective gain of 14 dBi. The AWG was set to sample the waveform at 6.125 GS/s and the spectrum analyzer captured complex I and Q samples at 200 MS/s. A center frequency of 2.4 GHz was selected for the test. It was noted prior to testing that a number of intermittent communications signals were operating within the bandwidth sampled by the spectrum analyzer.

The autocorrelation and cross-correlation of each of the 10^4 segments was first examined with the hardware in a loopback configuration. The cross-correlation was generated by correlating a given segment with the following segment. To provide an aggregated way in which to visualize the "goodness" of the waveform, the RMS average is computed across the set of segment autocorrelations and cross-correlations. The RMS average autocorrelation is shown in Figs. 2 and 3. The RMS average peak sidelobe level over the set of initial random segments is observed to be approximately –33 dB, which is improved to –43 dB by the spectral shaping optimization. Further, Fig. 3 reveals the presence of slight shoulder lobes for the initialization segments that have subsequently been smoothed out by a slight degradation in range resolution for the optimized segments. When the test set up was operated in a loopback configuration, the RMS average autocorrelation response of the captured waveform closely resembles that of the optimized waveform. The only non-conformity is an additional lower shoulder lobe present in positive delay (Fig. 3). This lobe was most likely produced by the lack of gain flatness in the spectrum analyzer's receive bandwidth.

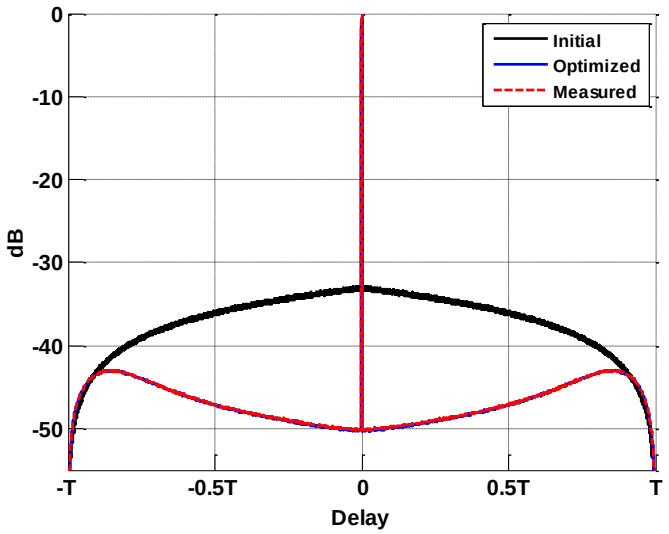

Fig. 2. RMS average autocorrelation response

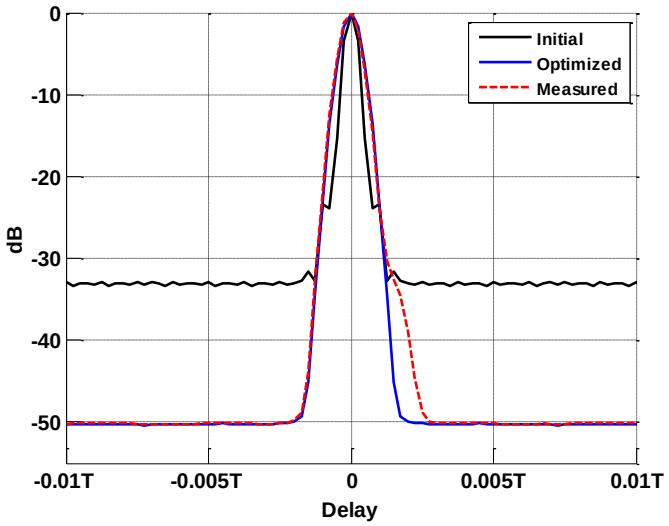

Fig. 3. RMS average autocorrelation response (mainlobe detail)

The RMS average cross-correlation of the segments is illustrated in Fig. 4. Compared to the initial segments, the spectral shaping optimization realizes a modest degradation for the cross-correlation maximum level from –33 dB to –31.5 dB. The measured cross-correlation response was nearly identical to the optimized response.

When performing Doppler processing over a set of segments the mainlobe response of each segment combines coherently while the sidelobe response does not, thereby producing sidelobe suppression in the autocorrelation as shown in Figs. 5 and 6. The mean sidelobe level for the coherently combined response is approximately 40 dB lower than the RMS average from Figs. 2 and 3 when all 10^4 segments are combined. The sidelobe response shown is only representative of that produced by a zero Doppler point scatterer. Any Doppler in the scatterer will produce a different sidelobe response, though it will still approximate the shape in Figs. 5 and 6.

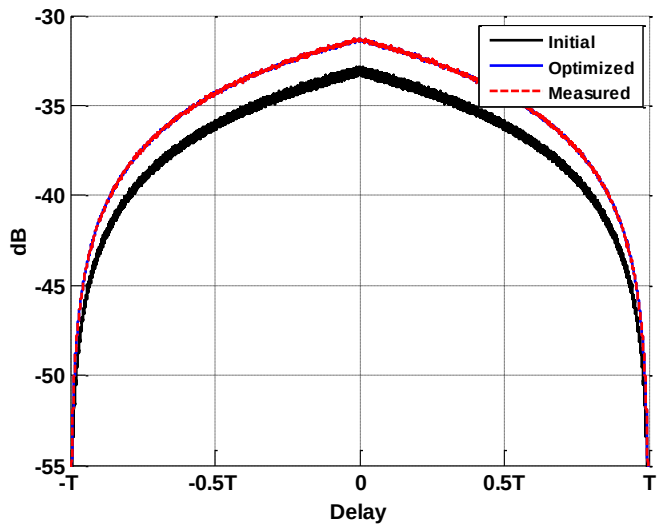

Fig. 4. RMS average cross-correlation response

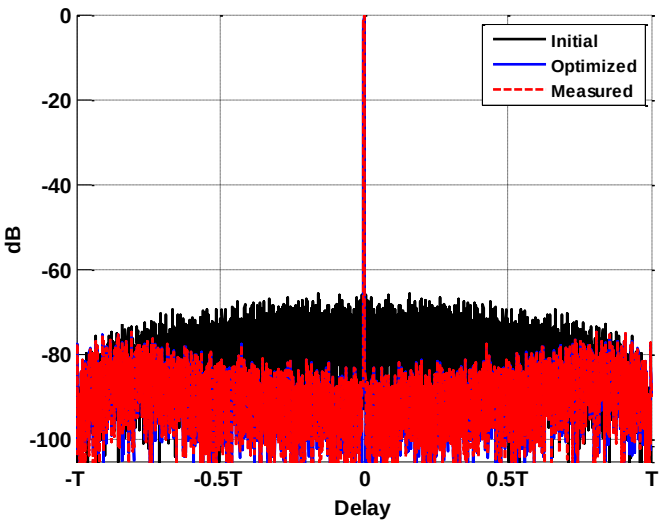

Fig. 5. Integrated autocorrelation response

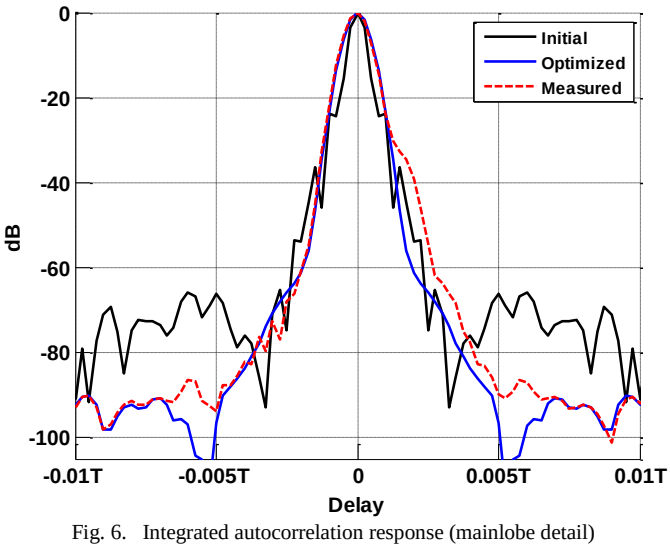

Fig. 6. Integrated autocorrelation response (mainlobe detail)

The sidelobe level of the optimized waveform is below –85 dB near the mainlobe and is below –75 dB towards the edge of the segment. A slight broadening of the mainlobe below –50 dB is evident when compared to the initial waveform (Fig. 6). The response of the measured waveform in loopback is very close to that of the optimized waveform. There again exists a slight shoulder lobe around –30 dB in positive delay, with an additional lobe produced at approximately –70 dB, that is again believed to be an artifact of the receive channel equalization.

The coherently combined cross-correlation response is shown in Figs. 7 and 8. The cross-correlation level of the optimized waveform is below –67 dB, and drops below –80 dB at the edges of the segment. While this response is at a satisfactory level, it is still above the integrated autocorrelation sidelobe level from Figs. 5 and 6. In this case, the cross-correlation is a measure of the sidelobes produced from range folded scatterers.

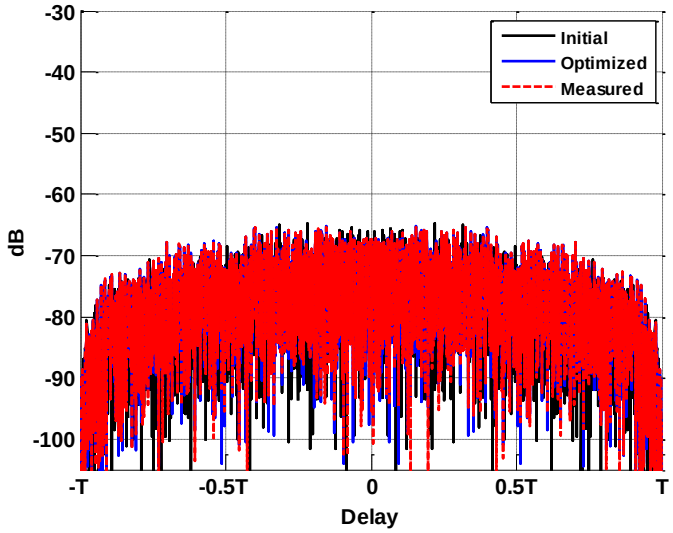

Fig. 7. Integrated cross-correlation response

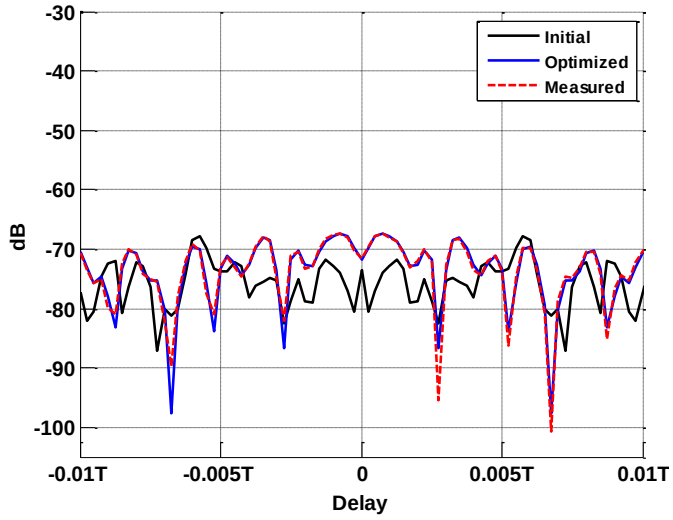

Fig. 8. Integrated cross-correlation response (detail)

The power spectral density (PSD) of each segment was computed and averaged with all other segments. This average PSD is shown in Fig. 9 for the initial waveform, the optimized waveform, and the measured loopback waveform. Also shown in Fig. 9 is the spectral shape used in the optimization process. It is evident that the initial waveform occupies a much larger bandwidth and has a more gradual spectral roll-off than the optimized waveform. The measured waveform has a sharp roll-off outside of twice the design bandwidth due to a maximum of 160 MHz analysis bandwidth for the spectrum analyzer. The mainlobe shape is slightly distorted as well due to the lack of channel equalization.

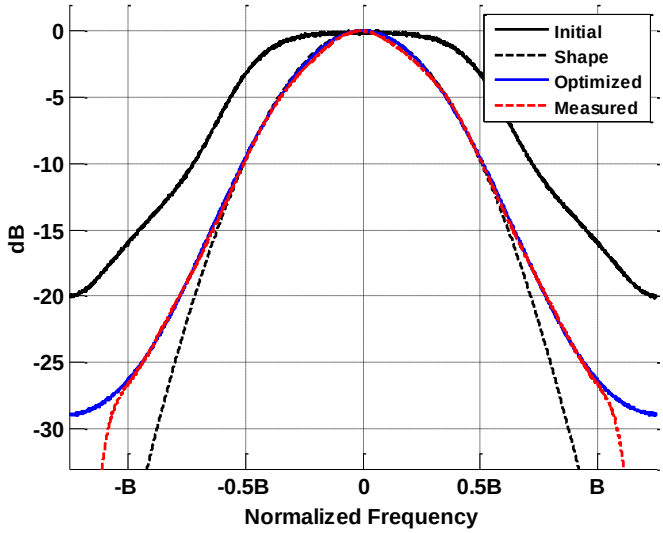

Fig. 9. Spectral content

To validate the loopback measurements, a laboratory test was performed in a room contained many large metal panels of varying shapes. The previously examined waveform was again used and was allowed to repeat continuously. The spectrum analyzer was used to capture 2 seconds of continuous data at the full 200 MS/s rate. A person walked towards the antennas while the system was operating. The last 50 nanoseconds of the previous segment and 2 microseconds of the following segment were included for matched filtering to capture all scatterers in the scene.

After matched filtering for each segment, the data was Doppler processed. A Blackman-Harris window was used to suppress Doppler sidelobes and a zero-Doppler projection filter was used to remove stationary clutter. This process only removed the mainlobe response of the clutter but left the sidelobe floor of the strongest scatterer intact. The range-Doppler map was normalized so that 0 dB corresponds to the strongest scatterer before clutter cancellation.

The range-Doppler map for the laboratory measurement is shown in Fig. 10. Note that the person is within 2 meters of the transmitter and that the room dimension is approximately 7 m. The moving target response is more than 60 dB above the surrounding sidelobe floor. There is also an abundance of reflections in the image that extend out past 3 times the room length due to multipath effects.

A Doppler velocity versus time plot is shown in Fig. 11. The range bin of the strongest scatterer from Fig. 10 is shown. The time axis has been interpolated with a sliding CPI window

using 10^4 segments. In Fig. 11 the micro-Doppler components of the walking person can be observed [16].

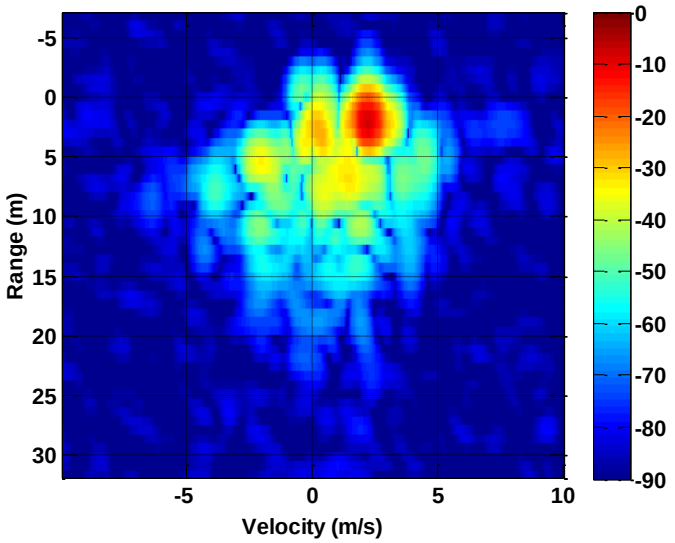

Fig. 10. Range-doppler map of a person walking

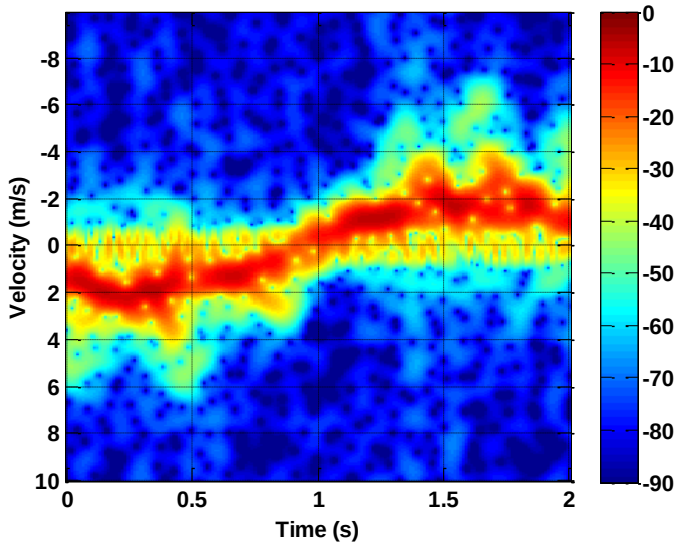

Fig. 11. Doppler velocity versus time

V. Free-Space Measurements

Finally, an open-air experiment was performed to verify the performance of the PRO-FMCW waveform. The same equipment used in the laboratory experiment was placed on the roof of a 3 story building located on the University of Kansas campus. Here the transmit and receive antennas were the vertical channels of two quad-ridged horn antennas. Each antenna provided about 10 dBi of gain. The center frequency was 2.3 GHz. A wideband amplifier with 27 dB of gain was selected which provided approximately 22 dBm of transmit power. The same 10^4 segments were transmitted and captured, yielding a total sampling time of 200 ms. For match filtering, the last 50 ns of the previous segment and 5 µs of the following segment were appended to the current segment thus allowing for a range profile of up to 750 meters. The equipment setup is shown in Fig. 12.

A map of potential scatterers is shown in Fig. 13. The range profile generated by the test is shown in Fig. 14. The conjectured scatterers in Fig. 13 are again labeled in Fig. 14. The apparent dynamic range of the integrated range profile response is at least 70 dB below the direct path interference peak, thereby allowing for a number of small scatterers to be observed.

Fig. 12. Equipment used for rooftop measurements

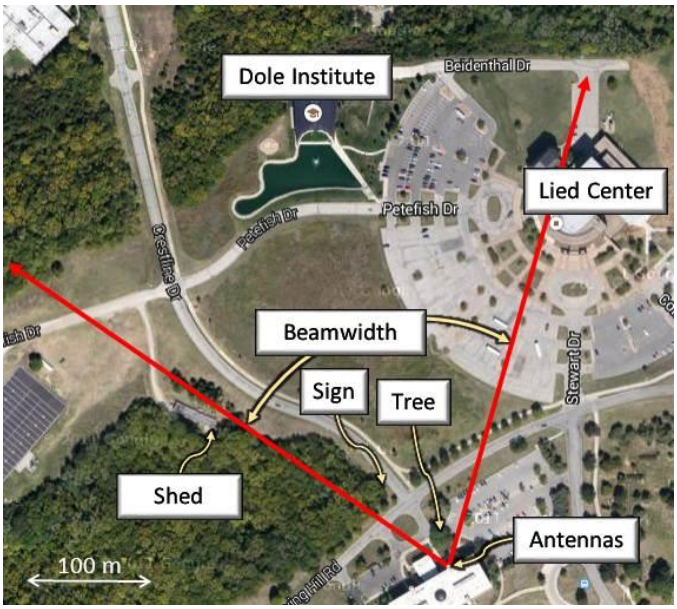

Fig. 13. Annotated map of radar scene

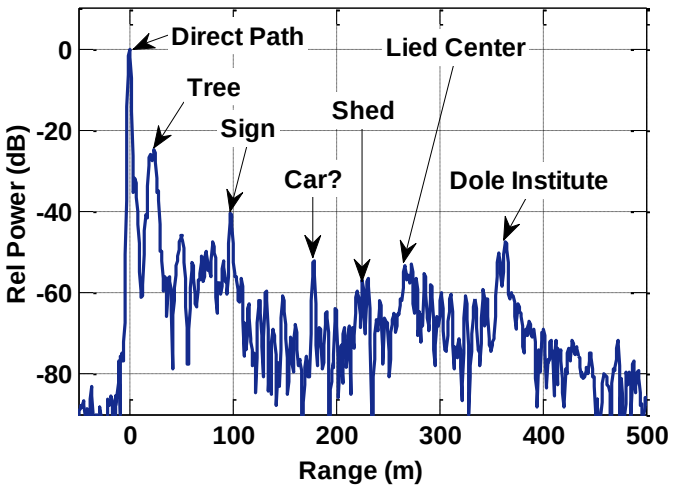

Fig. 14. Annotated range profile

The open-air test equipment was moved to the opposite side of the roof, and aimed at a road intersection about 1 km away. A dataset of 10^4 segments spanning 200 ms was again collected. Since the dynamic range of the data captured was limited by the large near-in scattering, the nearby scatterers were estimated using a least-squares formulation and subsequently subtracted from the measured data. The resulting range-Doppler map is shown in Fig. 15. The values depicted are normalized to the peak scatterer in the data without cancellation. Three moving targets with SINR greater than 10 dB were observed and are highlighted in red. All of the detected targets were below the –75 dB range-Doppler sidelobe level produced by the peak scatterer, which is why the cancellation stage was necessary. These moving targets are cars accelerating after a stoplight. Note that the speed limit of the road is 40 mph (approximately 18 m/s).

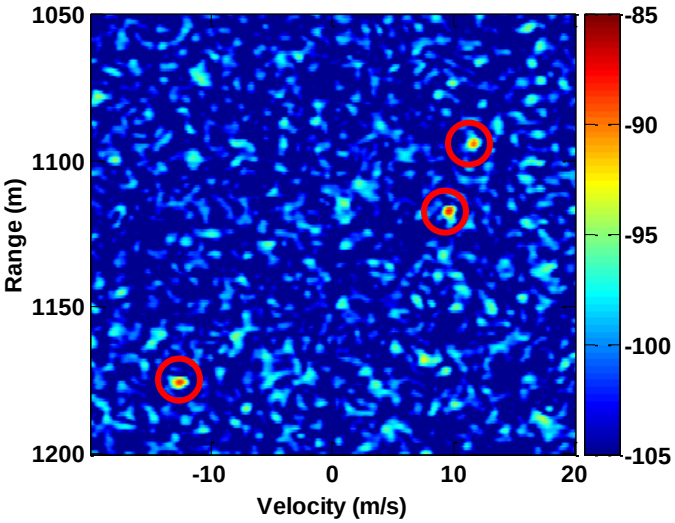

Fig. 15. Range-Doppler map of moving cars (dB scale)

VI. CONCLUSIONS

The design of a nonrecurrent, nonlinear FMCW waveform denoted as pseudo-random optimized (PRO-FMCW) was proposed that employs spectral shaping optimization. The waveform is divided into segments for optimization and range-Doppler receive processing. This waveform exhibits good spectral containment and was capable of producing range sidelobes below –75 dB. Following implementation using an arbitrary waveform generator and spectrum analyzer, physical measurements of a moving target (walking person) indicate sidelobe levels in the measured data that agree well with expectations. This performance was also verified using open-air measurements.

REFERENCES

[1] N. Levanon and E. Mozeson, *Radar Signals*, Wiley-IEEE Press, 2004.

[2] T. Higgins, K. Gerlach, A.K. Shackelford, and S.D. Blunt, "Aspects of non-identical multiple pulse compression," *IEEE Radar Conf.*, Kansas City, MO, pp. 895-900, 23-27 May 2011.

[3] D.P. Scholnik, "Range-ambiguous clutter suppression with pulse-diverse waveforms," *IEEE Radar Conf.*, Kansas City, MO, pp. 336-341, 23-27 May 2011.

[4] M. Cook, S.D. Blunt, J. Jakabosky, "Optimization of waveform diversity and performance for pulse-agile radar," *IEEE Radar Conf.*, Kansas City, MO, pp.812-817, 23-27 May 2011.

[5] S.D. Blunt, M.R. Cook, and J. Stiles, "Embedding information into radar emissions via waveform implementation," *Intl. Waveform Diversity & Design Conf.*, Niagara Falls, Canada, pp. 195-199, 8-13 Aug. 2010.

[6] T. Higgins, S.D. Blunt, and A.K. Shackelford, "Time-range adaptive processing for pulse agile radar," *Intl. Waveform Diversity & Design Conf.*, Niagara Falls, Canada, pp. 115-120, 8-13 Aug. 2010.

[7] M. Wicks, E. Mokole, S. Blunt, R. Schneible, and V. Amuso, eds., *Principles of Waveform Diversity and Design*, SciTech, 2010.

[8] U. Pillai, K.Y. Li, I. Selesnick, and B. Himed, *Waveform Diversity: Theory & Applications*, McGraw-Hill, 2011.

[9] F. Gini, A. De Maio, and L.K. Patton, eds., *Waveform Design and Diversity for Advanced Radar Systems*, IET, 2012.

[10] Special issue on "Signal Processing in Noise Radar Technology," *IET Radar, Sonar & Navigation*, vol. 2, no. 4, Aug. 2008.

[11] S.R.J. Axelsson, "Noise radar using random phase and frequency modulation," *IEEE Trans. Geoscience & Remote Sensing*, vol. 42, no. 11, pp. 2370-2384, Nov. 2004.

[12] T. Higgins, T. Webster, and A.K. Shackelford, "Mitigating interference via spatial and spectral nulls," *IET Intl. Radar Conf.* , 22-25 Oct. 2012

[13] W. Rowe, P. Stoica, and J. Li, "Spectrally constrained waveform design," *IEEE Signal Processing Magazine*, vol. 31, no. 3, pp.157-162, May 2014.

[14] J. Jakabosky, S.D. Blunt, and T. Higgins, "Ultra-low sidelobe waveform design via spectral shaping and LINC transmit architecture" *IEEE Intl. Radar Conf.*, Washington, DC, 11-15 May 2015.

[15] S.D. Blunt, M. Cook, J. Jakabosky, J. de Graaf, and E. Perrins, "Polyphase-coded FM (PCFM) radar waveforms, part I: implementation," *IEEE Trans. Aerospace & Electronic Systems*, vol. 50, no. 3, pp. 2218-2229, July 2014.

[16] V.C. Chen, F. Li, S.-S. Ho, and H. Wechsler, "Micro-Doppler effect in radar: phenomenon, model, and simulation study," *IEEE Trans. Aerospace & Electronic Systems*, vol. 42, no. 1, pp. 2-21, Jan. 2006.